

High-Resolution Chemical Identification of Polymer Blend Thin Films Using Tip-Enhanced Raman Mapping

Lijing Xue,^{*,†,‡} Weizhen Li,[†] Günter G. Hoffmann,^{†,‡} Johannes G. P. Goossens,[†] Joachim Loos,^{†,‡,§} and Gijsbertus de With[†]

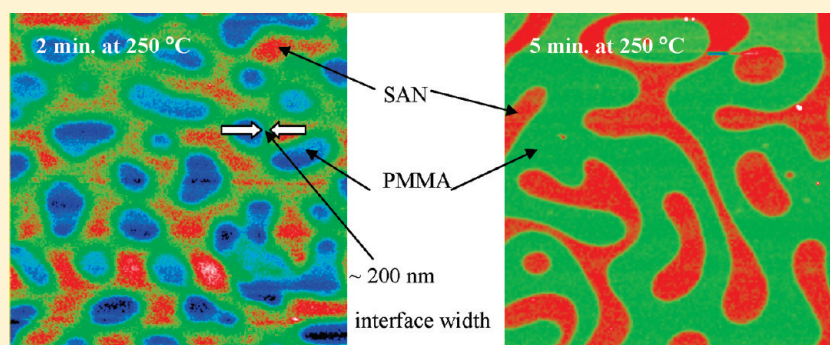
[†]Department of Chemical Engineering and Chemistry, Eindhoven University of Technology, P.O. Box 513, 5600 MB Eindhoven, The Netherlands

[‡]Dutch Polymer Institute, P.O. Box 902, 5600 AX Eindhoven, The Netherlands

[§]Department of Physics and Astronomy, University of Glasgow, Glasgow G12 8QQ, Scotland, United Kingdom

S Supporting Information

ABSTRACT:



Nanoscale chemical identification is required for the analysis of functional materials with fine structures. For the first time, high-resolution tip-enhanced Raman mapping (TERM) was applied to a polymer system: poly(methyl methacrylate) (PMMA)/poly(styrene-*co*-acrylonitrile) (SAN) thin films. Before TERM measurements were performed, the linear enhancement of tip-enhanced Raman spectroscopy (TERS) was optimized in terms of maximum Raman intensity. Up to 15 times of linear enhancement was obtained, as compared to the (conventional) confocal Raman intensity. The enhancement factor of TERS is greater than 1500 if taking the 100 times smaller probing area into account. As a result, a short exposure time was sufficient for high-resolution TERM measurements. Using TERM, the phase separation behavior of PMMA/SAN thin films was monitored by chemical recognition of local composition. The interface width (~ 200 nm) at the early stage of phase evolution was visualized. The comparison of TERM images at different stages of the phase separation process revealed an unexpected transition of PMMA from the dispersed phase to the continuous phase. This morphology transition of PMMA/SAN is briefly discussed in terms of the glass transition temperature, interface, and surface tension.

INTRODUCTION

Thin polymer blend films are widely used for coatings, packaging materials, barriers, membranes, sensors, and medical implants.^{1,2} The soft thin films are often mixtures of different polymers and additives. The miscibility of different types of polymers, the dispersion of the additives, and the network formation of the fillers are important factors for certain desired mechanical, thermal, and electrical conductivity properties. On the basis of miscibility, polymer blends can be classified as miscible, partially miscible, and immiscible. The miscibility/compatibility of different polymers influences the ultimate properties. For example, the adhesive strength between two polymer layers was found to increase linearly with the square root of interface width.³ For thin blend films, in particular, the interface width is essential to avoid mechanical failure and

thus to maintain the functional properties. Certain processing conditions, post-treatments, and addition of compatibilizers are required to obtain the desired morphology and to optimize interfacial interaction. The bulk morphology of partially miscible polymer blends can be tuned by controlled phase separation, via binodal or spinodal decomposition of thermodynamically metastable or unstable systems.⁴ Compared to the bulk systems, the phase evolution of thin films is far more complicated due to the confinement effect on thermodynamics, phase separation kinetics, and interfacial fluctuations.^{1,2,6–12} The spinodal decomposition of a poly(methyl methacrylate) (PMMA)/

Received: July 22, 2010

Revised: March 1, 2011

Published: March 23, 2011

poly(styrene-*co*-acrylonitrile) (SAN) blend has been studied experimentally and computationally using small-angle light scattering (SALS) and a diffuse-interface model, respectively.⁵ When the blend was annealed above the lower critical solution temperature (LCST), concentration fluctuation was found to be a dominant factor in the early stage of the phase separation.⁵ In the intermediate stage, the interface width was found to decrease and the correlation length to increase. In the late stage, a constant interface width was obtained and the correlation length was found to grow continuously. For thin films, the phase evolution and thus the morphology are dependent on parameters such as thickness, composition, temperature, viscosity, substrate, etc.^{1,2} To obtain insight into the phase separation behavior of the thin films, nondestructive characterizations of local morphology and chemical composition are equally important.

For morphology studies, atomic force microscopy (AFM) and transmission electron microscopy (TEM) are often used. For chemical identification of different phase domains, chemical etching and deuteration are required before AFM and forward recoil spectrometry measurements, respectively.

For nondestructive chemical analysis, better resolution can be obtained using confocal Raman, as compared to infrared (IR) and traditional Raman spectroscopy.^{13–20} The lateral resolution of conventional confocal Raman spectroscopy is dependent on the wavelength λ of the incident laser. This limitation makes it difficult to detect phase separation of small domains (<300 nm) and the extent of a phase separation as well as to judge the miscibility at the interface.

Thus, for fine structures at nanometer scale, local chemical identification with high spatial resolution is required. A recently developed technique, tip-enhanced Raman spectroscopy (TERS), provides such a possibility by combining scanning probe microscopy (SPM) and Raman spectroscopy.^{21–27} Above all, the lateral resolution of TERM is independent of the incident laser wavelength but is dependent on the radius of the tip. The enhancement of the Raman effect is due to the highly confined electromagnetic field of the laser at the tip, the surface plasmon on the sample, and the “lightning rod effect” from the tip.^{21–27} As a result, the probing volume of TERS is about $30 \times 30 \times 30 \text{ nm}^3$. Therefore, high-resolution chemical identification on a sample surface is possible using tip-enhanced Raman mapping (TERM).^{21,28} The detection sensitivity of TERS is improved compared to confocal Raman spectroscopy. It is hard to put a sensitivity limit on both confocal Raman and TERS methods, since the Raman sensitivity is different from one material to another and is highly dependent on their chemical nature. However, assuming a detection limit of 1% for confocal Raman spectroscopy and an enhancement factor of 2 for TERS, the detection limit should be about 0.5%. Note that the volume probed decreased by a factor of >3000. Previous TERS measurements have confirmed the surface enrichment of different components of a blend film at the air/polymer and the polymer/substrate interfaces.²¹ So far, no TERM on polymer systems was realized. It is difficult to maintain a constant TERS enhancement factor during a relatively long TERM measurement of a few days. A sharp tip with stable mechanical and chemical properties is of great importance.

In this work the phase separation behavior of a partially miscible PMMA/SAN (70/30 wt %) thin film was studied using TERS. For the first time, nondestructive chemical mapping was carried out using TERM as well. Spin-coated uniform PMMA/SAN films with a thickness of about 500 nm were annealed above the LCST to induce phase separation. The treated films showed

visible domains of different sizes under optical microscopy. The enhancement of the TERS signal was first optimized in terms of the maximum Raman intensity, with respect to the intensity of confocal Raman spectra recorded at the same position on the sample. The phase separation behavior of the films was then studied using high-resolution TERM. The TERM images at different stages were compared to obtain new insights into the phase separation behavior of the PMMA/SAN blend films.

EXPERIMENTAL SECTION

Sample Preparation. Materials similar to those in ref 5 were used. The number-average molecular weight (M_n), polydispersity (PDI), and glass transition temperature (T_g) of both PMMA (Arkema, France) and SAN of 28 wt % acrylonitrile (Dow Chemical Company, The Netherlands) are listed in Table 1. PMMA and SAN were dissolved in methyl ethyl ketone (MEK, Merck) at a weight ratio of 70 to 30, which is the critical ratio for the bulk system.⁵ The solution was filtered, spin-coated on glass slides, and dried in a vacuum oven at 150 °C for 5 h. The typical film thickness was $\sim 500 \text{ nm}$.

Table 1. Molecular Characteristic Information of PMMA and SAN

polymer	M_n	PDI	$T_g/^\circ\text{C}$	$\delta/(\text{J}^{1/2}/\text{cm}^{3/2})$	$\gamma^{\text{Cal}}/(\text{mJ}/\text{m}^2)$
PMMA	42 000	2.1	~ 120	$18.9^a (18.6\text{--}26.2)^b$	42.5
SAN	41 000	2.2	~ 115	21.9^a	47.7

^a Calculated value. ^b Experimental range.³⁰

Demixing/phase separation was then induced by post-treatment using a heating stage preheated to 250 °C (above the LCST of 203 °C). Films I and II were heated for 2 and 5 min, respectively, and then quenched to room temperature directly.

Tip Preparation. The acid solution for etching was prepared by mixing absolute ethanol (p.A., Merck) and 37% HCl (p.A., Merck) at a volume ratio of 1:1. A 99.999% gold wire (Alfa) of 200 μm diameter was flame annealed before etching. A cone-shaped gold tip, with a typical radius of $\sim 30 \text{ nm}$, was prepared by electrochemical etching with an applied voltage of 2.4 V as described in the literature.^{22,29}

Measurement. Optical microscopy, TERS, and TERM measurements were carried out using an NTEGRA SPECTRA (NT-MDT, Russia). A scanning near-field optical microscopy head (SNLG101NTF, NT-MDT, Russia) was placed above an inverted optical microscope (Olympus IX70). A self-etched gold tip, a 100 \times oil immersion objective (Olympus, NA = 1.3, refractive index of oil $n = 1.516$), a pinhole of 40 μm , and a continuous wave linearly polarized He–Ne laser (633 nm) were used for all measurements. The tip was aligned to the focus of the laser before any TERS/TERM measurement, as described in our previous report.²² The TERS or confocal Raman measurements were optimized in terms of the maximum Raman intensity when the tip was approached or was withdrawn from the sample surface. The enhancement factor was different from tip to tip, depending on the shape and the radius of the tip, and the distance between the tip and the sample. To ensure nondestructive measurements, a low laser power (<100 μW , on the sample) was used. For the same reason, a lower laser power was set for TERS and TERM measurements of a higher enhancement factor. A typical lateral/depth resolution of about 20–30 nm is expected from these measurements.²¹

RESULTS AND DISCUSSION

The PMMA and SAN polymers selected are similar to the materials used in ref 5. The number-average molecular weight (M_n), polydispersity (PDI), and glass transition temperature (T_g) are shown in Table 1.

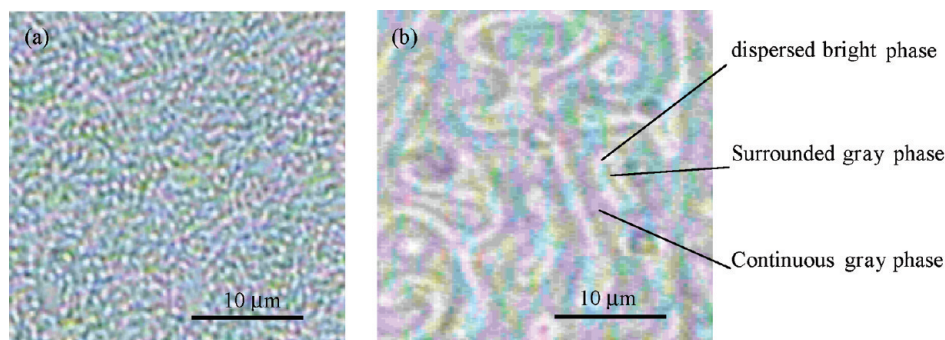


Figure 1. Optical microscopy images ($30\ \mu\text{m} \times 30\ \mu\text{m}$) of the PMMA/SAN blend films, using bright-field mode. (a) Film I and (b) film II were annealed at $250\ ^\circ\text{C}$ for 2 and 5 min, respectively.

The blend thin films were prepared at a weight ratio of 70/30 by spin-coating. The solubility parameters of both polymers were calculated using

$$\delta = (E_{\text{Coh}}/V)^{1/2} \quad (1)$$

where δ , E_{Coh} , and V are the solubility parameter, the molar cohesive energy, and the molar volume.³⁰ As shown in Table 1, the calculated solubility parameter values of SAN ($21.9\ \text{J}^{1/2}/\text{cm}^{3/2}$) and PMMA ($18.9\ \text{J}^{1/2}/\text{cm}^{3/2}$) are similar. Moreover, the calculated value for PMMA was within the experimental range of $18.6\text{--}26.2\ \text{J}^{1/2}/\text{cm}^{3/2}$.³⁰ Therefore, a uniform blend of PMMA and SAN can be produced. The films, heated at $150\ ^\circ\text{C}$ for 5 h, indeed did not show any phase separation. At elevated temperature ($>203\ ^\circ\text{C}$) phase separation occurred. Figure 1 shows the optical microscopy images of films I and II, heated at $250\ ^\circ\text{C}$ for 2 and 5 min, respectively. A difference in domain size can be clearly observed between the two films. Compared to the relatively irregular and large phase domains in film II, the phase domains in film I appears to be dotlike and wormlike. In both cases, the dispersed phase domains appear brighter than the continuous phase. The morphology of film II is more complex than that of film I, with an additional gray phase surrounded by the dispersed bright phase. It is interesting to know whether the chemical composition of the surrounded gray phase is different from that of the continuous gray phase.

Confocal Raman, TERS, and TERM Measurements on Film II. The confocal Raman spectra were first recorded on film II, when the laser beam was focused on the bright and the continuous gray phases as shown in Figure 1. The spectra are compared in Figure 2. The laser power at the sample was less than $100\ \mu\text{W}$, and the exposure time was 120 s. The bright phase was identified as SAN due to the characteristic Raman bands at 1002 and $1600\ \text{cm}^{-1}$, corresponding to the stretching vibrations of the phenyl ring, as well as at $2240\ \text{cm}^{-1}$ corresponding to the stretching vibration of the $\text{C}\equiv\text{N}$ bond.^{31,32} The continuous gray phase is identified as PMMA due to the characteristic Raman band at $800\ \text{cm}^{-1}$ corresponding to the stretching $\text{C}\text{--}\text{C}$ vibration.^{31,32}

Therefore, it is possible to analyze the local chemical composition of different phases by monitoring the Raman intensity at 800 and $1002\ \text{cm}^{-1}$ corresponding to the PMMA and SAN components. A shear force scanning probe head equipped with a self-etched gold tip was then positioned on top of the sample stage. The tip was approached to the film surface and aligned to the focus of the laser by tip scans, as described previously.²² The TERS and confocal Raman spectra were recorded at the same position on the sample. The same laser power and exposure time

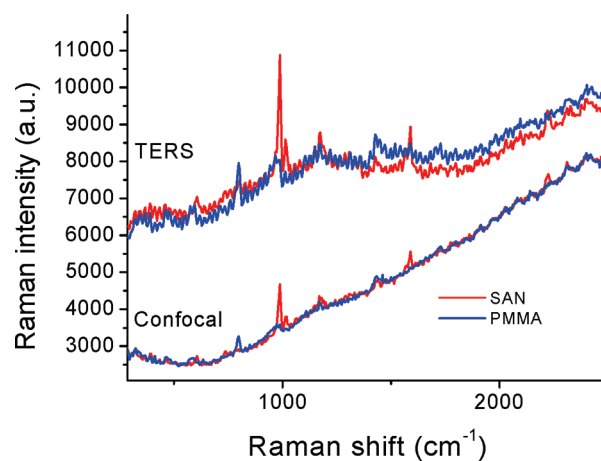


Figure 2. Comparison of TERS and confocal spectra, recorded at $100\ \mu\text{W}$ for 120 s. The spectra of SAN (in red) and PMMA (in blue) were recorded when the laser is focused on the dispersed bright phase and the continuous gray phase shown in Figure 1b.

were set here for both measurements. The comparison between the TERS and the confocal Raman spectra of SAN (in red) and PMMA (in blue) domains is shown in Figure 2. An enhancement factor of 3 was achieved in the TERS mode, in terms of the maximum Raman intensity of characteristic Raman bands. If taking the different probing area into account, an enhancement factor of >300 was obtained in this case.

Systematic studies on SAN33/PMMA films^{6–12} showed a PMMA wetting layer on the film surface. If that were the case in our system, a stronger enhancement should be observed for PMMA than for SAN, since the nearer the sample to the tip, the stronger the enhancement.²² Surprisingly, the same enhancement factor for PMMA and SAN was obtained. This indicates that PMMA and SAN are approximately equally close to the tip. Therefore, we suggest there was no obvious surface enrichment of PMMA at the air/polymer interface in our system.

The differences between the two systems as listed in Table 2 probably lead to the difference in phase evolution behavior.

TERM measurement was then performed using a stage scan over an area of $30\ \mu\text{m} \times 30\ \mu\text{m}$ using 150×150 points, which corresponds to a nominal pixel size of $200\ \text{nm}$. The exposure time was set to $10\ \text{s}/\text{point}$. The TERM images of SAN and PMMA in terms of the maximum Raman intensity at 1002 and $800\ \text{cm}^{-1}$ are displayed in Figure 3a,b. From these figures we conclude that the phase in red (Figure 3a) is SAN-rich and the

phase in green (Figure 3a) is PMMA-rich, corresponding to the bright and the continuous gray phases in Figure 1b, respectively. The surrounded gray phase in Figure 1b was found to have the same chemical composition as the dispersed bright phase. An atomic force microscopy (AFM) measurement shows a height difference of ~ 70 nm across film II.³³ This indicates that the contrast as observed using optical microscopy is probably due to the roughness of the film but not the difference in chemical composition.

No PMMA characteristic Raman band was observed in the SAN phase in both the confocal Raman and TERS spectra, and vice versa. This suggests a pseudo-2D phase separation, since confocal Raman spectroscopy measures up to $1\text{--}3\ \mu\text{m}$ in depth and our films are only ~ 500 nm thick. It also indicates that the early stage concentration fluctuation was finished within 5 min, at $250\ ^\circ\text{C}$. Figure 3 suggests either a bicontinuous phase distribution or, at least partially, a single phase dispersed in another. Actually, whether phases are bicontinuous can only be properly judged from 3-D information. Hence for this stage we denote the phases as SAN-rich and PMMA-rich in semibicontinuous morphology. The TERM images of film II match well with the AFM images of the regime labeled D for the SAN33/PMMA system¹² in an intermediate stage of phase separation. The area covered by PMMA was calculated to be $63 \pm 10\%$ in Figure 3b and that covered by SAN to be about $36 \pm 10\%$ in Figure 3a, using the software of our spectrometer.

Confocal Raman, TERS, and TERM Measurements on Film I. The optimized TERS spectrum of film I annealed for 2 min was compared with the corresponding confocal Raman spectrum in Figure 4. There was a 15 times enhancement in terms of the maximum Raman intensity and more than 1500 times taking the different probing area into account. Because of the 5 times higher enhancement factor compared to the previous TERS on film II, a lower laser power was set for film I. TERM was then performed

Table 2. Comparison between SAN33/PMMA¹² and the Present SAN28/PMMA System

current system (SAN28/PMMA)	SAN33/PMMA ¹²
SAN28 (28% AN)	SAN33 (33% AN)
T_g (PMMA) $\sim 120\ ^\circ\text{C}$	T_g (PMMA) $\sim 105\ ^\circ\text{C}$
glass, rough	silicon, flat
fast phase separation (in min)	slow phase separation (in h)

over an area of $10\ \mu\text{m} \times 10\ \mu\text{m}$ using 256×256 points, with a nominal pixel size of $40\ \text{nm}$. The exposure time was set to $5\ \text{s}/\text{point}$. The TERM images of SAN and PMMA are shown in Figure 5a,b. The Raman intensity increases as indicated by the scale bar, from black via blue and green to red. Different from film II, the dispersed phase was found to be PMMA-rich and the continuous phase SAN-rich, corresponding to the bright and the gray phases in Figure 1a, respectively. We noticed a broad boundary region between the continuous and the dispersed phases, appearing in green in both TERM images in Figure 5. This indicates a PMMA–SAN interphase at the interfacial region of the SAN-rich and PMMA-rich domains.

Compared with the clear contrast in phases of film II, the phase contrast in TERM images of film I was less pronounced (Figure 5). This indicates that phase separation was in the early stage, where the diffusion of different components is playing an important role.⁵ For the analysis of the interface width and the local chemical composition of each phase, TERM at higher resolution is required. A high-resolution TERM measurement was then carried out at the boundary region of film I with a nominal pixel size smaller than $8\ \text{nm}$ (128×128 points for the $1\ \mu\text{m} \times 1\ \mu\text{m}$ scanning area). An average interface width of $179\ \text{nm}$ with a mean deviation of $20.8\ \text{nm}$ was obtained from data analysis at 10 different places in Figure 6a. The interface width of about $200\ \text{nm}$ is in reasonable agreement with the estimated value of $150\ \text{nm}$ from the SALS measurements for early stage phase

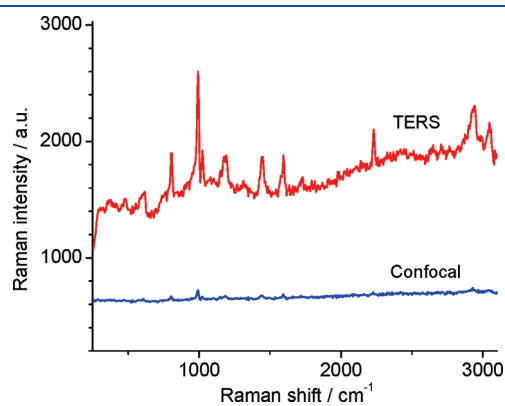


Figure 4. Comparison of TERS (in red) and confocal (in blue) Raman spectra of film I, annealed at $250\ ^\circ\text{C}$ for 2 min.

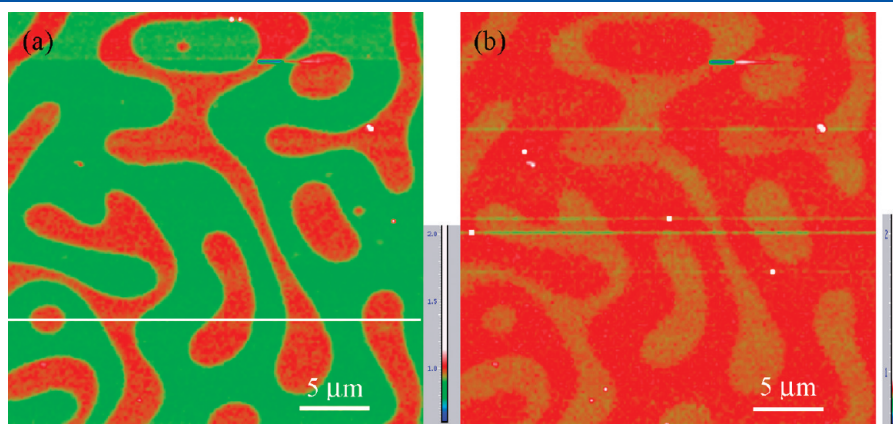


Figure 3. TERM in terms of the maximum Raman intensity of the Raman bands (a) at $1002\ \text{cm}^{-1}$ corresponding to SAN and (b) at $800\ \text{cm}^{-1}$ corresponding to PMMA on film II. Annealed at $250\ ^\circ\text{C}$ for 5 min. The Raman intensity profile along the white line in (a) is shown in Figure 7.

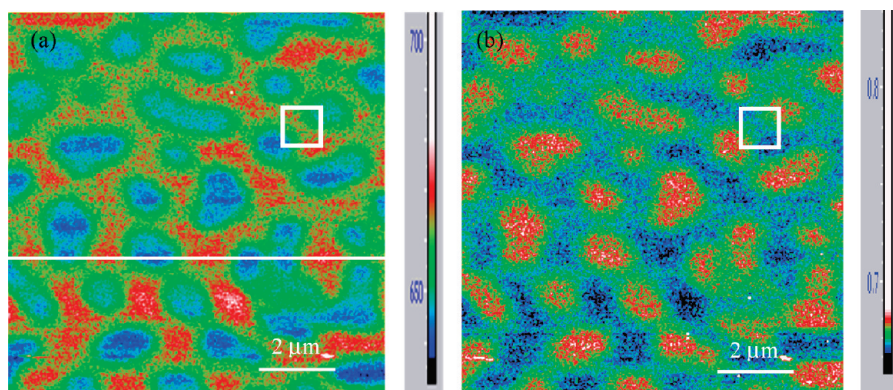


Figure 5. TERM in terms of the maximum Raman intensity of the Raman bands (a) at 1002 cm^{-1} corresponding to SAN and (b) at 800 cm^{-1} corresponding to PMMA on film I, annealed at $250\text{ }^{\circ}\text{C}$ for 2 min. The Raman intensity profile along the white line in (a) is shown in Figure 7.

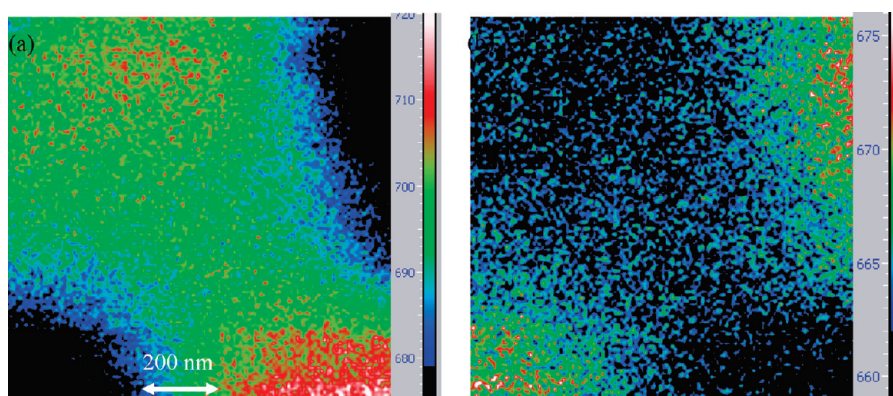


Figure 6. TERM at the boundary region between two phases as indicated in Figure 5 in terms of the maximum Raman intensity of the Raman bands (a) at 1002 cm^{-1} corresponding to SAN and (b) at 800 cm^{-1} corresponding to PMMA on film I. The arrow indicates the interface width between SAN and PMMA phases.

separation.⁵ This interphase probably ensures a good adhesion between different phase domains. Above all, PMMA was found to be present in the SAN-rich phase, as shown in Figure 6b. The interphase shows a continuous concentration gradient from one to the other polymer domains. However, it should be kept in mind that both the limited probing depth ($<30\text{ nm}$) and the surface constraint may influence the measurement of the interface width. Such influence is negligible in the case of film I. The maximum height difference on film I is less than 10 nm .³³ This is far smaller than the transition boundary region ($>200\text{ nm}$).

Estimating the Flory–Huggins interaction parameter χ from the interfacial width, degree of polymerization, and average segment length (see Supporting Information³³) yields $\chi \cong 0.003$ while the χ value as estimated from solubility parameters³⁰ yields a much higher value ($\chi \cong 0.179$). This indicates that the system is not in equilibrium yet, consistent with the much smaller interfacial width of about $30\text{--}40\text{ nm}$ for PMMA/SAN systems at equilibrium.³

Comparison between the Phase Separation Behavior of Films I and II. In Figure 7, the sizes of SAN domains in films I and II are compared. In film I, the continuous SAN-rich phase appeared to be $1.0\text{--}1.5\text{ }\mu\text{m}$ in size at the cross section. It is somewhat smaller than the initial average value of $1.8\text{ }\mu\text{m}$ for the bulk system.⁵ This again indicates an early stage phase separation. Because of the slightly lower T_g of SAN as compared with PMMA, the mobility of SAN chains is higher than that of PMMA

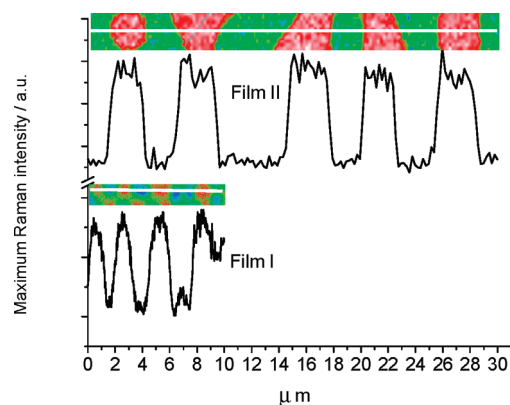


Figure 7. Raman intensity profile at 1002 cm^{-1} corresponding to SAN along the white lines in Figures 3a and 5a.

chains. Phase separation of the PMMA/SAN mixture proceeds via the formation of a SAN-rich continuous phase and a PMMA-rich dispersed phase. In film II, the SAN domains were found to have grown in size up to $3\text{--}4\text{ }\mu\text{m}$, indicating an intermediate stage.

An unexpected morphology transition of PMMA-rich phase, from a dispersed phase into a continuous phase, was found. The SAN continuous phase was also found to break down. This might

indicate a higher surface energy of SAN than that of the PMMA phase. Hence, the surface tension of both components was estimated based on group contributions using

$$\gamma = (P_s/V)^4 \quad (2)$$

where γ , P_s , and V are the surface tension, the molar parachor, and the molar volume, respectively.³⁰ As shown in Table 1, the estimated surface tension of SAN is about 48 mJ/m², slightly higher than that of PMMA about 43 mJ/m². Therefore, the phase inversion of PMMA/SAN is likely due to the higher surface energy of SAN as compared to PMMA.

Though the surface energy of PMMA is lower than that of SAN, no obvious surface enrichment of PMMA at the air/polymer interface was observed. The interfacial tension γ_{12} was calculated using

$$\gamma_{12} \approx (\gamma_1^{1/2} - \gamma_2^{1/2})^2$$

where γ_1 and γ_2 are the surface tensions for PMMA and SAN, respectively.³⁰ The resulting value of about 0.15 mJ/m² is far lower than that of the reported system (1 mJ/m² for SAN33/PMMA³⁴).

The phase evolution kinetics of the current system was found different from that of the SAN33/PMMA.¹² In our case, the high surface energy component SAN has a lower T_g (~115 °C) so that phase separation is likely to proceed via the formation of a SAN-rich continuous phase. Because the interfacial energy of the SAN/PMMA is only 0.15 mJ/m², this process is not too much hampered and the structure is kinetically determined in film I. After longer annealing time, thermodynamics takes over so that a morphology change occurs as shown in film II, yielding a similar morphology as reported in ref 12. We speculate that with a large interfacial energy and a low T_g of the low surface energy component the bicontinuous morphology (film II) may appear directly or much faster, as reported for the systems mentioned in ref 12.

CONCLUSION

For the first time TERM measurements on an important class of synthetic polymer materials (a PMMA/SAN blend) was realized. Using a cone-shaped gold tip, up to 15 times linear enhancement was achieved, as compared to conventional confocal Raman spectroscopy. The enhancement factor is greater than 1500 times when the 100 times smaller probing area is taken into account.

Besides the high spectral sensitivity of TERS, we were able to reveal information on the local chemical composition of the blend films by applying TERM with nanoscale resolution. Moreover, the improved detection sensitivity of TERS and TERM allows the detailed chemical analysis at the interface/interphase region, such as the measurement interface width and the concentration gradient of each component.

The comparison of TERM images at different phase separation stages revealed a phase inversion of the PMMA/SAN blend. At the early stage of the phase separation, PMMA and SAN were the dispersed and the continuous phases, respectively. This probably indicates a better mobility of the SAN due to its lower T_g as compared to PMMA. A change to semibicontinuous morphology occurs after a few minutes at 250 °C. This might be due to the precise balance of interface and surface energies of both components.

The results unambiguously show the power of TERS and TERM for advanced chemical analysis of complex systems with nanoscale resolution.

ASSOCIATED CONTENT

S Supporting Information. AFM height images of films I and II. Estimation of the Flory–Huggins interaction parameter χ . This material is available free of charge via the Internet at <http://pubs.acs.org>.

AUTHOR INFORMATION

Corresponding Author

*E-mail L.xue@tue.nl. Tel +31 (0)40 2473132, fax +31 (0)40 2445619.

ACKNOWLEDGMENT

We are grateful for the financial support by Dutch Polymer Institute (DPI) (grant #692) and technical support by NT-MDT.

REFERENCES

- Wang, H.; Composto, R. J. *Macromolecules* **2002**, *35*, 2799–2809.
- Liao, Y.; Su, Z.; Ye, X.; Li, Y.; You, J.; Shi, T.; An, L. *Macromolecules* **2005**, *38*, 211–215.
- Stamm, M.; Schubert, D. W. *Annu. Rev. Mater. Sci.* **1995**, *25*, 325–356.
- Utracki, L. A. *Commercial Polymer Blends*; Chapman & Hall: London, 1998.
- Prusty, M.; Keestra, B. J.; Goossens, J. G. P.; Anderson, P. D. *Chem. Eng. Sci.* **2007**, *62*, 1825–1837.
- Chung, H. J.; Taubert, A.; Deshmukh, R. D.; Composto, R. J. *Europhys. Lett.* **2004**, *68*, 219–225.
- Chung, H. J.; Composto, R. J. *Phys. Rev. Lett.* **2004**, *92*, 185704.
- Wang, H.; Composto, R. J. *J. Chem. Phys.* **2000**, *113*, 10386–10397.
- Wang, H.; Composto, R. J. *Phys. Rev. E* **2000**, *61*, 1659–1663.
- Newby, B. Z.; Composto, R. J. *Macromolecules* **2000**, *33*, 3274–3282.
- Wang, H.; Composto, R. J. *Europhys. Lett.* **2000**, *50*, 622–627.
- Chung, H. J.; Wang, H.; Composto, R. J. *Macromolecules* **2006**, *39*, 153–161.
- Huan, S.; Lin, W.; Sato, H.; Yang, H.; Jiang, J.; Ozaki, Y.; Wu, H.; Shen, G.; Yu, R. *J. Raman Spectrosc.* **2007**, *38*, 260–270.
- Schmidt, U.; Hild, S.; Ibach, W.; Hollricher, O. *Macromol. Symp.* **2005**, *230*, 133–143.
- Schmidt, P.; Dybal, J.; Šćudla, J.; Raab, M.; Kratochvil, J. *Macromol. Symp.* **2002**, *184*, 107–122.
- MacDonald, A. M.; Vaughan, A. S.; Wyeth, P. *Appl. Spectrosc.* **2003**, *57*, 1475–1481.
- Merino, J. C.; del, M.; Fernández, R.; Pastor, J. M. *Macromol. Symp.* **2001**, *168*, 55–65.
- Schmidt, P.; Kolařík, J.; Lednický, F.; Dybal, J.; Lagarón, J. M.; Pastor, J. M. *Polymer* **2000**, *41*, 4267–4279.
- Quintanilla, L.; Rodríguez-Cabello, J. C.; Jawhari, T.; Pastor, J. M. *Polymer* **1994**, *35*, 514–518.
- Schmidt, P.; Fernandez, M. R.; Pastor, J. M.; Roda, J. *Polymer* **1997**, *38*, 2067–2075.
- Yeo, B.-S.; Amstad, E.; Schmid, T.; Stadler, J.; Zenobi, R. *Small* **2009**, *5*, 952–960.
- Kharintsev, S. S.; Hoffmann, G. G.; Dorozhkin, P. S.; de With, G.; Loos, J. *Nanotechnology* **2007**, *18*, 315502.
- Novotny, L.; Stranick, S. J. *Annu. Rev. Phys. Chem.* **2006**, *57*, 303–331.

- (24) Pettinger, B.; Ren, B.; Picardi, G.; Schuster, R.; Ertl, G. *J. Raman Spectrosc.* **2005**, *36*, 541–550.
- (25) Richards, D.; Milner, R. G.; Huang, F.; Festy, F. *J. Raman Spectrosc.* **2003**, *34*, 663–667.
- (26) Stöckle, R. M.; Suh, Y. D.; Deckert, V.; Zenobi, R. *Chem. Phys. Lett.* **2000**, *318*, 131–136.
- (27) Hartschuh, A.; Beversluis, M. R.; Bouhelier, A.; Novotny, L. *Philos. Trans. R. Soc. London, A* **2004**, *362*, 807–819.
- (28) Steidtner, J.; Pettinger, B. *Phys. Rev. Lett.* **2008**, *100*, 236101.
- (29) Ren, B.; Picardi, G.; Pettinger, B. *Rev. Sci. Instrum.* **2004**, *75*, 837.
- (30) van Krevelen, D. W.; Hoftyzer, P. J. *Properties of Polymers, Their Estimation and Correlation with Chemical Structure*; Elsevier Scientific Publishing Company: Amsterdam, 1976; p 162.
- (31) Nishimoto, M.; Keskkula, H.; Paul, D. R. *Polymer* **1989**, *30*, 1279–1286.
- (32) Suess, M.; Kressler, J.; Kammer, H. W. *Polymer* **1987**, *28*, 957–960.
- (33) See Supporting Information.
- (34) Chung, H. J.; Ohno, K.; Fukuda, T.; Composto, R. J. *Nano Lett.* **2005**, *5*, 1878–1882.